The past, present and future of the heavier electroweakinos in the light of LHC and other data

Amitava Datta[1] **and Nabanita Ganguly**

Department of Physics, University of Calcutta,
92 Acharya Prafulla Chandra Road, Kolkata 700009, India

E-mail: adatta_ju@yahoo.co.in, nabanita.rimpi@gmail.com

ABSTRACT: The aim of this paper is to showcase the novel multilepton ($nl + \not{E}_T$, n = 3–5) signals, hitherto unexplored at the LHC, arising from the heavier electroweakinos, in several generic pMSSMs at the upcoming LHC experiments. We first briefly review our old constraints on the full electroweakino sector of these models, containing both lighter and heavier sparticles, using the ATLAS trilepton data from the LHC Run I. Next we derive new stronger constraints on this sector for the first time using the ATLAS Run II data. We identify some benchmark points and explore the prospect of observing multilepton events in future LHC experiments. Our focus is on the channels with $n > 3$ which are the hallmarks of the heavier electroweakinos. If the spectrum of the lighter electroweakinos is compressed, these signals might very well be the discovery channels of the electroweakinos at the high luminosity LHC. We also discuss the implications of the new LHC constraints for the observed dark matter relic density of the universe, the measured value of the anomalous magnetic moment of the muon and the dark matter direct detection experiments.

KEYWORDS: Supersymmetry Phenomenology

---

[1]INSA Senior Scientist.

Contents

1 Introduction

Supersymmetry (SUSY) is a novel symmetry which predicts that corresponding to every boson (fermion) in the Standard Model (SM) there is a fermionic (bosonic) superpartner which are collectively called the sparticles (For reviews and text books on supersymmetry, see, e.g., [1–4] and [5, 6] respectively). The painstaking searches for the sparticles spanning several years at the LHC Run I and Run II experiments are approaching the next long shutdown. Yet no signal has been seen so far. This leads to stringent lower bounds on many sparticle masses [7, 8]. As expected the bounds on the masses of the strongly interacting sparticles (the squarks and the gluinos) with large production cross-sections turn out to be the most stringent ones. In some models the relevant limits could be as large as 2–3 TeV. Therefore the possibility that the masses of these sparticles could be beyond the kinematic reach of the LHC is gradually gaining ground.

If this indeed is the case then the best bet for SUSY discovery is to search for the spin-1/2 sparticles belonging to the electroweak (EW) sector. These superpartners of the gauge and Higgs bosons are called the electroweakinos (eweakinos). As a sequel to our earlier works [9, 10], we wish to highlight in this paper the novel multilepton ($nl + \not{E}_T$, n = 3,4,5) signals arising from the heavier ones among the eweakinos in several generic models at the upcoming LHC experiments. It may be stressed that the signals for $n > 3$ are hallmarks of the heavier eweakinos as the strength of these signals are rather poor if they are decoupled. Moreover, if the lighter eweakinos have a compressed spectrum these could very well be eweakino discovery channels.

It is worth recalling that the LHC collaborations have so far executed dedicated searches in the trilepton channel targeting the lighter eweakinos using both Run I [11–14] and Run II [15, 16] data. As is well known model independent mass limits are hard to extract from the current data since the signals depend on too many unknown parameters (mostly the soft SUSY breaking terms) present in the most general Minimal Supersymmetric Standard Model (MSSM). Thus the LHC collaborations usually derive the constraints from the search results in the so called simplified models [11–16]. These models may be obtained after imposing some simplifying assumptions on the general MSSM which reduce the number of free parameters. Decoupling of the heavier eweakinos is one of the many ad hoc assumptions thus invoked.

The above limits were reexamined [17, 18] in the phenomenological MSSM (pMSSM) [19] with 19 free parameters. It has been shown that in some regions of the parameter space the predictions of the pMSSM resemble that of the simplified models employed by the ATLAS group quite well and the resulting limits are very similar (for comparisons using Run I and Run II data, see figure 1 of [17], figure 7, 8 of [20] and figure 1 of this paper). In several other regions, however, the limits in the pMSSMs are significantly weaker. However, the decoupling of heavier eweakinos was also assumed in these papers. In fact most of the recent analyses involving the eweakinos [21–25] also imposed the ad hoc assumption that the heavier eweakinos are decoupled.

The heavier eweakinos were included in the analyses of [9, 10, 26, 27] using the LHC Run I data and very recently in [28] using the LHC Run II data. In the detailed analyses of [9, 10] it was pointed out that the non-decoupled heavier eweakinos may have three important implications for the LHC searches.

- The ATLAS and CMS collaborations have interpreted the null search results from the $3l + \not{E}_T$ signal in various simplified models with decoupled heavier eweakinos. The main results of their analyses are exclusion contours in the $m_{\widetilde{\chi}_1^\pm} - m_{\widetilde{\chi}_1^0}$ plane. On the other hand in a pMSSM with non-decoupled heavier eweakinos similar constraints may become significantly stronger due to the additional contributions from the heavier eweakinos to the signal (see figures 3, 4 and 5 of [10] based on the ATLAS Run I data). This, however, is a quantitative change.

- There are qualitatively new results as well. The cascade decays of the heavier eweakinos can lead to novel multilepton (n-lepton (l) + $\not{E}_T$, n = 3,4,5) signals. It may be recalled that events with $n > 3$ are not very common in the models with decoupled heavier eweakinos.

- If the lighter eweakinos have a compressed mass spectrum, the signals from the heavier ones could even be the SUSY discovery channels. For example, the conventional trilepton signals ($n = 3$) which dominantly come from the former may be swamped by the SM background while signals with $n > 3$ triggered by the latter, which have highly suppressed backgrounds, may show up at the LHC.

The last two points were illustrated in section 6 of [10].

It should be emphasized that the interest in the eweakino sector is not restricted to LHC signatures alone. These sparticles can shed light on the origin of the observed Dark Matter (DM) in the Universe [29, 30],[1] improve the agreement between the measured anomalous magnetic moment of the muon (a_μ) [44, 45] and the theoretical prediction [46, 47]. Last but not the least, the naturalness [48–51] of any SUSY model favours small values of the EW parameter μ known as the higgsino mass parameter. The constraints on this parameter from the LHC searches and other observables can , therefore, potentially test various SUSY models in the light of naturalness arguments.

In this paper we update and upgrade the constraints in [9, 10] using, for the first time, the LHC Run II data (ATLAS) and other non LHC constraints, taking into account all eweakinos — the heavier as well as the lighter ones. We then define a set of post LHC Run II benchmark points (BPs) and use them to assess the prospect of observing the multilepton signatures in future high luminosity LHC experiments after the next long shut down.

The plan of this paper is as follows. In section 2 we present a brief discussion of different pMSSMs involving both heavier and lighter eweakinos studied in this work. The models are summarized in table 1 and the choice of parameters for scanning in each case is listed after this table. The methodology adopted to get the main results are described in detail in section 3. In section 4 we identify the allowed parameter space (APS) of the models discussed in section 2 in the light of LHC data from Run II, the observed value of DM relic density of the universe and also the experimental constraint from the measured value of the anomalous magnetic moment of muon. The prospect of observing various multilepton signals in different models is assessed using post LHC Run II BPs selected from the corresponding APS. In section 5 we check the status of all models introduced in section 2 vis-a-vis the spin-independent DM direct detection cross-section limits. Finally we conclude in section 6.

2 The pMSSMs to be constrained

In this section we briefly review several pMSSMs with 19 parameters [19] which are then constrained using the LHC eweakino search at Run II and other data in a later section. We emphasize that these models are generic in the sense that different models are characterized by certain hierarchies among the masses and mass parameters rather than their specific values. The fermionic sparticles in the EW sector are the charginos ($\widetilde{\chi}_j^\pm$, $j = 1, 2$) and the neutralinos ($\widetilde{\chi}_i^0$, $i = 1 - 4$) — collectively called the eweakinos. The indices i and j are arranged in ascending order of masses. The masses and compositions of these sparticles are

---

[1]For reviews and recent phenomenological works see e.g., [31–43].

determined by four parameters: the U(1) gaugino mass parameter M_1, the SU(2) gaugino mass parameter M_2, the higgsino mass parameter μ and $\tan\beta$ — the ratio of the vacuum expectation values of two neutral Higgs bosons. If no assumption regarding the SUSY breaking mechanism is invoked, the soft breaking masses M_1, M_2 and the superpotential parameter μ are all independent. Throughout this paper we take $\tan\beta = 30$ since relatively large values of this parameter give a better agreement with the a_μ data, ensure that the SM like Higgs boson has practically the maximum mass at the tree level and improve the prospect of charged Higgs boson search. The stable, neutral lightest neutralino ($\widetilde{\chi}_1^0$), which is assumed to be the lightest supersymmetric particle (LSP), is a popular DM candidate.

The scalar sparticles are the L and R type sleptons which are superpartners of leptons with left and right chirality. The sneutrinos are the superpartners of the neutrinos. We assume L(R)-type sleptons of all flavours to be mass degenerate with a common mass $m_{\widetilde{l}_L}(m_{\widetilde{l}_R})$. Because of the SU(2) symmetry the sneutrinos are mass degenerate with L-sleptons modulo the D-term contribution. We neglect L-R mixing in the slepton sector. For simplicity we work in the decoupling regime (see e.g., [52]) of the Higgs sector with only one light SM like Higgs boson, a scenario consistent with all Higgs data collected so far (See e.g., [53]).

The signals of the eweakinos at the LHC are also sensitive to their compositions which are governed by the hierarchy among the parameters M_1, M_2 and μ. Most of the existing analyses revolve around the broad scenarios listed in the next few subsections.

Following our earlier works [9, 10, 17, 18] we introduce a convenient nomenclature with four letters for denoting the pMSSMs belonging to three broad scenarios. The first two letters represent the composition of the lighter eweakinos which lead to the signals when the heavier ones are decoupled. We have considered three generic cases: the LW (Light Wino) model ($M_2 \ll \mu$), the LH (Light Higgsino) model ($M_2 \gg \mu$) and the LM (Light Mixed) model ($M_2 \approx \mu$). These models will be described in subsections 2.1, 2.2 and 2.3 respectively. In subsection 2.4 we shall consider a few LH models where the lighter eweakino spectrum is compressed in different ways and the observable signals are mainly due to the heavier eweakinos.

2.1 The LW models ($M_2 \ll \mu$)

In this class of models the two relatively light and nearly degenerate eweakinos ($\widetilde{\chi}_1^\pm$ and $\widetilde{\chi}_2^0$) are wino like and their masses are controlled by the parameter M_2. They are the main sources of the signal/signals. The production cross-section of the higgsino like heavier eweakinos ($\widetilde{\chi}_2^\pm$, $\widetilde{\chi}_3^0$ and $\widetilde{\chi}_4^0$), with masses controlled by the parameter μ, are suppressed both due to their composition and larger masses. Thus their contributions to the signal are negligible. The assumption that the heavier eweakinos are decoupled is therefore realistic in this case. Here the LSP is either a pure bino ($M_1 \ll M_2$) or a wino-bino admixture ($M_1 \approx M_2$). The trilepton signal ($3l + \not{E}_T$) in this model also depend sensitively on the hierarchy among the sleptons and the eweakino masses. This leads to the following subclasses:

- LWLS (Light Wino Light Left Slepton) model (1.1 a).

- LWHS (Light Wino Heavy Slepton) model (1.1 b).

The simplified model considered by the LHC collaborations [11–16] with wino dominated $\widetilde{\chi}_1^\pm$ and $\widetilde{\chi}_2^0$, bino dominated $\widetilde{\chi}_1^0$ and decoupled heavier eweakinos is a special case of this generic pMSSM in the limit of very large μ.

In the LWLS model (1.1 a) only the left sleptons ($\widetilde{l}_L$) are lighter than $\widetilde{\chi}_1^\pm$ and $\widetilde{\chi}_2^0$ while the right sleptons ($\widetilde{l}_R$) are assumed to be decoupled. These eweakinos directly decay into sleptons and sneutrinos via two body modes with large branching ratios (BRs) which enhances the leptonic signals. Sleptons belonging to all generations are assumed to be degenerate and their common mass lies between $m_{\widetilde{\chi}_1^0}$ and $m_{\widetilde{\chi}_1^\pm}$. The choice $m_{\widetilde{l}_L} = (m_{\widetilde{\chi}_1^\pm} + m_{\widetilde{\chi}_1^0})/2$ by the LHC collaborations optimizes the leptonic signals and yields the strongest bounds on the lighter eweakino masses (see section 3.2, figure 1). In later section we shall mostly use this choice of $m_{\widetilde{l}_L}$ whenever this sparticle is assumed to be light. However, one can also think of various tilted scenarios where $m_{\widetilde{l}_L}$ is either shifted towards $m_{\widetilde{\chi}_1^0}$ or $m_{\widetilde{\chi}_1^\pm}$ so that the eweakino spectrum is somewhat compressed leading to weaker but not drastically different mass limits if the compression is not extreme. Several tilted models were examined in the light of LHC Run I data and other constraints [17].

In the LWHS (1.1 b) model all sleptons ($\widetilde{l}_L$ and $\widetilde{l}_R$) are heavier than $\widetilde{\chi}_1^\pm$ and $\widetilde{\chi}_2^0$. These eweakinos decay into leptonic final states only via (on-shell or off-shell) W and Z bosons respectively. Since the BRs of leptonic W and Z decays are small, the leptonic signals in this case are suppressed compared to the LWLS model leading to weaker bounds on $m_{\widetilde{\chi}_1^\pm}$. The LHC collaborations have published mass limits in a simplified model related to this scenario assuming decoupled heavier eweakinos [15, 16]. Multilepton signals are not favoured in these LW type models. However we will briefly discuss in a later section that these are one of those few models which are consistent with the current DM direct detection data [54–56] taken at its face value.

2.2 The LH models ($M_2 \gg \mu$)

In this class of models the relatively light higgsino like eweakinos are $\widetilde{\chi}_1^\pm$, $\widetilde{\chi}_2^0$ and $\widetilde{\chi}_3^0$ with masses controlled by the parameter μ. They are the main sources of the signal/signals if the heavier eweakinos are decoupled. The pair production cross-sections of these higgsino like eweakinos are small compared to that in the LW models for comparable masses of the lighter eweakinos. Thus weaker mass bounds are obtained from the LHC data. In all cases the LSP is either a pure bino ($M_1 \ll \mu$) or a bino-higgsino admixture ($M_1 \approx \mu$). The constraints on this model using the Run I data were obtained in [18].

It should be stressed that the wino dominated heavier eweakinos ($\widetilde{\chi}_2^\pm$ and $\widetilde{\chi}_4^0$) are phenomenologically important in this scenario. Their masses are determined by the free parameter M_2. As expected the pair production cross-sections of these eweakinos are suppressed due to their larger masses. However, their favourable couplings to the gauge bosons compensate this suppression to some extent. As a result their contributions to the signals turn out to be appreciable or even dominant when the lighter eweakino spectrum is compressed. This point was emphasized in [9, 10] and the importance of the heavier eweakinos was illustrated using the LHC RUN I data. We have constrained the following models using Run II and other data in this paper:

- The LHLS (Light Higgsino Light Left Slepton) model (2.2 a).

- The LHHS (Light Higgsino Heavy Slepton) model (2.2 b).

In the former model the L-slepton — lighter eweakino mass hierarchies are similar to that in the LWLS model (see subsection 2.1). In the LHHS model it is assumed that all sleptons are heavier than the lighter eweakinos ($\widetilde{\chi}_1^\pm$, $\widetilde{\chi}_2^0$ and $\widetilde{\chi}_3^0$) but are lighter than the heavier eweakinos. In the numerical computations the common slepton mass is chosen to be $m_{\tilde{l}_L} = m_{\tilde{l}_R} = (m_{\widetilde{\chi}_1^\pm} + m_{\widetilde{\chi}_2^\pm})/2$ and we set $M_2 = 1.5\mu$. An additional attraction of the LHHS model is that it is consistent with the DM direct detection data [54–56] as will be shown in a later section.

2.3   The LM models ($M_2 \approx \mu$)

Here all eweakinos except the LSP are wino-higgsino admixtures. The LSP is dominantly a pure bino but in some zones of the parameter space all eweakinos are admixtures of all the weak eigenstates. In [10] the LMLS model was constrained using the LHC Run I data. In this paper we have updated these constraints using the LHC Run II data.

2.4   The compressed LHHS models

In this section we consider a few LHHS models (2.2 b) where the lighter eweakinos have a compressed spectrum. As a result observable multilepton signals come mainly from the heavier eweakinos. We consider the following models:

- The CLHHS ($\widetilde{W}$) (Compressed Light Higgsino Heavy Slepton) model with wino ($\widetilde{W}$) like heavier eweakinos [9, 10] (2.4 a).

- The MCLHHS ($\widetilde{W}$): same as (2.4 a) except that the light higgsinos are moderately compressed [10] (2.4 b).

- The CLHHS ($\widetilde{B} - \widetilde{W}$) model with one bino ($\tilde{B}$) like and one wino ($\tilde{W}$) like heavier eweakino (2.4 c).

In the CLHHS ($\widetilde{W}$) model we set $M_1 \simeq \mu$ with $M_2 > \mu$. This choice leads to a compressed lighter eweakino spectrum where $\widetilde{\chi}_1^0$, $\widetilde{\chi}_2^0$, $\widetilde{\chi}_3^0$ and $\widetilde{\chi}_1^\pm$ are approximately mass degenerate and each has significant bino and higgsino components. The masses of the wino dominated heavier eweakinos are determined by the free parameter M_2. As in all LHHS models we set $m_{\tilde{l}_L} = m_{\tilde{l}_R} = (m_{\widetilde{\chi}_1^\pm} + m_{\widetilde{\chi}_2^\pm})/2$ so that the sleptons are always heavier than lighter eweakinos. For future use we define a compression parameter $x = \mu/M_1$ which represents the degree of compression. For numerical results in the CLHHS ($\widetilde{W}$) model we have chosen $x = 1.05$.

As discussed in detail in sections 5.1 and 6.5 of [10], the compatibility of CLHHS ($\widetilde{W}$) model with the observed DM relic density is obtained for $m_{\widetilde{\chi}_2^\pm} > 600\,\text{GeV}$. On the other hand in the MCLHHS ($\widetilde{W}$) model with slightly larger value of x ($= 1.3$) this compatibility is obtained for lower values of $m_{\widetilde{\chi}_2^\pm}$ which ensure better signals. In [10] this issue was illustrated with some BPs. Here we make a detailed study of the phenomenology of this

Model	Hierarchies among	Compositions of eweakinos		
Name	mass parameters	LSP	Lighter eweakinos	Heavier eweakinos
LHLS (see model (2.2 a))	$M_1 < M_{\tilde{l}} < \mu < M_2$	Bino	Higgsino	Wino
LHHS (see model (2.2 b))	$M_1 < \mu < M_{\tilde{l}} < M_2$	Bino	Higgsino	Wino
LMLS (see subsection 2.3)	$M_1 < M_{\tilde{l}} < M_2 \approx \mu$	Higgsino	Wino-higgsino	Wino-higgsino
CLHHS ($\widetilde{W}$), MCLHHS ($\widetilde{W}$) (see models (2.4 a) and (2.4 b))	$M_1 \approx \mu < M_{\tilde{l}} < M_2$	Bino-higgsino	Bino-higgsino	Wino
CLHHS ($\widetilde{B} - \widetilde{W}$) (see model (2.4 c))	$\mu < M_{\tilde{l}} < M_1 = M_2$	Higgsino	Higgsino	Bino, Wino

Table 1. Hierarchies among mass parameters for different models described in detail in section 2. The compositions of eweakinos in each case are also shown.

model by making a parameter space scan using the constraints from LHC Run II and other data.

The CLHHS ($\widetilde{B} - \widetilde{W}$) model with non-decoupled heavier eweakinos have higgsino like and nearly degenerate $\widetilde{\chi}_1^0$, $\widetilde{\chi}_2^0$, $\widetilde{\chi}_3^0$ and $\widetilde{\chi}_1^\pm$. As a result the signals from the lighter eweakinos are expected to consist of only soft visible particles. For a long time there was no LHC constraint on this model. More recently both ATLAS [57] and CMS [58] collaborations have obtained some interesting constraints on simplified models closely related to this model using improved techniques for detecting soft leptons [59]. The excluded parameter space corresponds to $m_{\widetilde{\chi}_1^0} \approx m_{\widetilde{\chi}_1^\pm} = 100\text{--}140\,\mathrm{GeV}$. A comparison with figure 5 of [18] shows that in a closely related pMSSM such masses may be theoretically forbidden. In this paper we focus on scenarios with non-decoupled heavier eweakinos. Here $\widetilde{\chi}_2^\pm(\widetilde{\chi}_4^0)$, $\widetilde{\chi}_3^0$ are chosen to be wino and bino dominated respectively or admixtures of these components. Then multilepton signals can directly come from the production and decay of these sparticles.

2.5 Summary of parameter spaces in different pMSSMs and the method of scanning

We summarize the mass parameter hierarchy and the corresponding compositions of eweakinos in table 1 for each pMSSM discussed in this section:

In order to carry out the parameter space scanning in each pMSSM to obtain the LHC limits, the following choices have been made for free and fixed parameters:

- *LHLS Model:* in this case the scanning is done over M_1 and μ while M_2 and $M_{\tilde{l}}$ are fixed by $M_2 = 1.5\,\mu$ and $M_{\tilde{l}} = (m_{\widetilde{\chi}_1^0} + m_{\widetilde{\chi}_1^\pm})/2$ respectively.

- *LHHS Model:* the choice of parameters for LHHS model is exactly same as in LHLS model. The only difference is in the choice of slepton mass parameter which is taken as $M_{\tilde{l}} = (m_{\widetilde{\chi}_1^\pm} + m_{\widetilde{\chi}_2^\pm})/2$ in this case.

- *LMLS model:* in this case M_1 and M_2 are taken as free parameters. M_2 and μ are very closely spaced and are related by the choice $\mu = 1.05\,M_2$. Sleptons lie between the LSP and the lighter eweakinos with the specific choice $M_{\tilde{l}} = (m_{\widetilde{\chi}_1^0} + m_{\widetilde{\chi}_1^\pm})/2$.

- *CLHHS ($\widetilde{W}$) and MCLHHS ($\widetilde{W}$) models:* here we take M_1 and μ to be related by $\mu = xM_1$ where x is taken as 1.05 for extreme compression (CLHHS ($\widetilde{W}$)) and 1.3 for moderate compression (MCLHHS ($\widetilde{W}$)). The scanning is performed over M_1 and M_2 while the slepton mass parameter $M_{\tilde{l}}$ is taken as the arithmetic mean of $m_{\widetilde{\chi}_1^\pm}$ and $m_{\widetilde{\chi}_2^\pm}$.

- *CLHHS ($\widetilde{B} - \widetilde{W}$) model:* for this type of model, μ and M_1 (which is degenerate with M_2) are free parameters. $M_{\tilde{l}}$ is a dependent parameter which is related to eweakino masses via the relation $M_{\tilde{l}} = (m_{\widetilde{\chi}_1^\pm} + m_{\widetilde{\chi}_2^\pm})/2$.

3 Methodology

The work in this paper is based on the following methodology.

3.1 The constraints

We first constrain the pMMSMs discussed in the previous section using the model independent ATLAS Run II data in the $3l + E\!\!\!/_T$ channel collected with $36.1\,\text{fb}^{-1}$ of integrated luminosity [16]. We have also used the ATLAS Run II constraints from slepton search data [16] when the model under consideration contains a light slepton. The constraint on the CLHHS ($\widetilde{B} - \widetilde{W}$)[2] also takes into account the ATLAS higgsino search data using the soft lepton detection technique [57]. However we have not simulated the last two signals. Instead we have simply rejected the points lying within the ATLAS exclusion contours.

We have also used the WMAP/Planck constraints [29, 30] and that from the measured value of the anomalous magnetic moment of the muon [44, 45] following the discussions of [10]. We believe that the theoretical and experimental uncertainties in the above three constraints are relatively small. To clarify this statement further we note that the constraints from flavour physics can be applied to the MSSM only after imposing yet another assumption known as the minimal flavour violation. In a nutshell this implies that the mixing angles in the squark and quark sectors are the same. For a discussion on non-minimal flavour violation , see for example, ref [60].

We have also taken into consideration the constraints from different experiments on direct detection of the DM [54–56]. As is well known this data disfavours many SUSY models. However there are many assumptions, both theoretical and experimental, in the derivation of the spin-independent LSP-nucleon scattering cross-section σ_{SI} (for a brief discussion see, e.g, section 4 of [10] and the references there in). Relaxing these assumptions may significantly lower the computed value of σ_{SI}. This makes the comparison of the theoretical prediction and the experimental upper bound on σ_{SI} somewhat ambiguous. We have, therefore, not displayed the impact of these constraints in our main figures. They are discussed in a separate section.

3.2 The simulation

Using PYTHIA we simulate the $3l + E\!\!\!/_T$ events in the pMSSMs studied by us. We closely follow the ATLAS group for selection and isolation of signal objects [16]. Jets are reconstructed

---

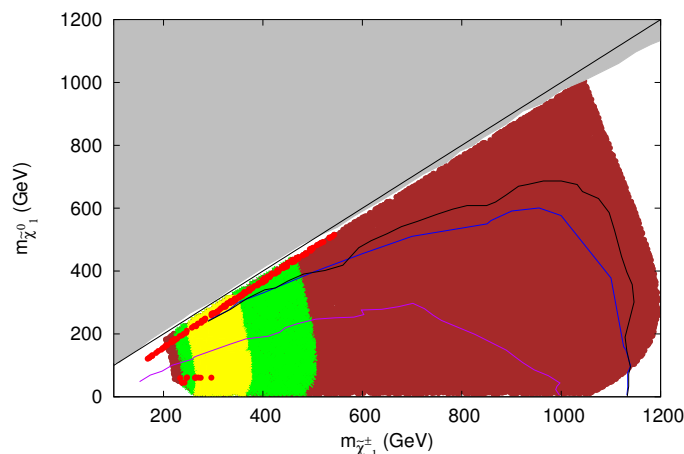[2]See model (2.4 c) of subsection 2.4.

Figure 1. The black line represents the exclusion contour in the $m_{\widetilde{\chi}_1^\pm} - m_{\widetilde{\chi}_1^0}$ plane at 95% CL in a simplified model (see text) obtained by the ATLAS collaboration from trilepton searches at 13 TeV LHC [16]. The blue line shows the exclusion obtained by our simulations in the closely related LWLS model. The area enclosed by the magenta curve is excluded by the ATLAS slepton search at Run II (see text). The brown, green and yellow regions are consistent with the a_μ data at 3σ, 2σ and 1σ levels respectively. The red points satisfy WMAP/PLANCK data of the DM relic density. The grey region at the upper left corner is disfavoured theoretically.

using the anti-k_T [61] algorithm with radius parameter R = 0.4 and they have $p_T > 20$ GeV, $|\eta| < 2.8$. Signal e and μ are required to have $p_T > 10$ GeV and $|\eta| < 2.47$ (2.5) for e (μ). ATLAS has defined 11 signal regions (SRs) each characterized by a set of cuts. Some of these regions target slepton mediated decays of $\widetilde{\chi}_1^\pm$ and $\widetilde{\chi}_2^0$ while others target W and Z mediated decays. The results are presented in terms of number of observed events in the $3l + \not{E}_T$ channel in each SR and the corresponding number of SM backgrounds (see table 13 and 14 of [16]) extracted from the data. With these two numbers one can obtain the model independent upper bound on N_{BSM} for each SR [62]. We have used this information to constrain the pMSSMs discussed in the last section. In figure 1 we compare the exclusion contours obtained by us and the one by the ATLAS collaboration from the Run II trilepton search data [16]. They had obtained the contour for a simplified model with wino like $\widetilde{\chi}_1^\pm$ and $\widetilde{\chi}_2^0$ and a bino like LSP with light sleptons (the black exclusion contour). The pMSSM closest to the above simplified model is the LWLS model (see subsection 2.1, model (1.1 a)) with decoupled heavier eweakinos. The blue exclusion contour in figure 1 is the result of our simulation in this model. It may be noted that for $m_{\widetilde{\chi}_1^\pm} \gg m_{\widetilde{\chi}_1^0}$, $\widetilde{\chi}_1^\pm$ ($\widetilde{\chi}_1^0$) is almost a pure wino (bino) and the results of these two simulations agree quite well. As $m_{\widetilde{\chi}_1^0}$ increases, $\widetilde{\chi}_1^\pm$ ($\widetilde{\chi}_2^0$) acquires significant bino component. As a result the $\widetilde{\chi}_1^\pm \widetilde{\chi}_2^0$ production cross-section decreases leading to weaker exclusions. Each point in the parameter space corresponds to a L-slepton mass due to the choice $m_{\widetilde{l}_L} = (m_{\widetilde{\chi}_1^0} + m_{\widetilde{\chi}_1^\pm})/2$. The magenta curve is the exclusion contour from the ATLAS slepton search data at Run II.

The impact of the other two constraints — namely the measurements of a_μ and the DM relic density as discussed in section 3.1 are also shown by different colour bands. The colour convention is explained in the figure caption. It may be noted that the APS consistent

with all constraints is rather tiny. As we shall show in the next section the APSs in some of the LH models are considerably larger.

We next turn our attention to the prospect of observing multilepton signals ($nl + \displaystyle{\not}E_T$ with n = 3,4,5) for an integrated luminosity of $3000\,\text{fb}^{-1}$. From the APS of each pMSSM with non-decoupled heavier eweakinos we select a few BPs. We then simulate the signals corresponding to each BP for different n. We closely follow different selection criteria introduced in the ATLAS Run II analysis [16]. The estimation of the SM background for each n is common to all pMSSMs studied here. They will be presented in the next section.

All signals in this work are generated using PYTHIA [63]. The relevant background processes in case of $nl + \displaystyle{\not}E_T$ with $n > 3$ are generated using ALPGEN [64] with MLM matching [65, 66] and then passed through PYTHIA for showering and hadronization. Jets are reconstructed using FASTJET [67] with anti-k_T algorithm. For parton distribution function (PDF), CTEQ6L [68] has been used in all our simulations.

3.3   Scanning of the parameter spaces

The squark mass parameters, M_A, M_3 which do not play any role in our present simulation are set at a large value of $2\,\text{TeV}$. The trilinear coupling A_t is fixed at $-2\,\text{TeV}$ so that the Higgs mass m_h falls within the experimentally allowed window $122\,\text{GeV} < m_h < 128\,\text{GeV}$ around a central value of $125\,\text{GeV}$ [69, 70]. All other trilinear couplings are set at zero. The heavier Higgs like bosons are assumed to be decoupled. For all our simulations, we have fixed $\tan\beta$ at 30 which gives better agreement with a_μ data and the parameters M_1, M_2, μ are varied (for the details see subsection 2.5 and table 1). The masses of sleptons are fixed by the definition of each model as discussed in section 2. The SM Parameters are taken as follows: $m_t^{pole} = 175\,\text{GeV}$, $m_Z = 91.18\,\text{GeV}$, $m_b^{\overline{ms}} = 4.2\,\text{GeV}$ and $m_\tau = 1.77\,\text{GeV}$. The complete SUSY spectrum and a_μ are evaluated using SuSpect [71]. The decay modes of sparticles are calculated using SUSY-HIT [72]. We compute the DM relic density and σ_{SI} using micrOMEGAs [73].

4   Results

In this section, we perform detail scanning of the parameter space of each of the generic model described in section 2 subjected to three constraints — ATLAS eweakino search data in the $3l + \displaystyle{\not}E_T$ channel at the LHC Run II, the observed DM relic density of the universe and the experimentally measured anomalous magnetic moment of the muon and identify the APS for each of them. We then discuss the prospects of discovery for these models through various multilepton channels for an integrated luminosity of $3000\,\text{fb}^{-1}$. We specifically emphasize on the $nl + \displaystyle{\not}E_T$ channel with $n > 3$ that arises predominantly from the non-decoupled heavier eweakinos.

We begin by estimating the SM backgrounds to all multilepton signals in subsection 4.1. Since the three compressed models introduced in section 2 nicely highlight the importance of the heavier eweakinos, we first discuss the phenomenology of these models (see subsections 4.2, 4.3 and 4.4). The following subsections deal with the remaining models.

Channel	Cuts
$4l + \not{E}_T$	$N_l = 4,\ m_{\mathrm{SFOS}} \notin (81.2, 101.2)\,\mathrm{GeV},\ \not{E}_T > 80\,\mathrm{GeV},\ n_{b-jet} = 0$
$ss3os1l + \not{E}_T$	$N_l = 4$ with $Q_l \neq 0,\ \not{E}_T > 80\,\mathrm{GeV}$
$5l + \not{E}_T$	$N_l = 5,\ \not{E}_T > 80\,\mathrm{GeV}$

Table 2. The different choices of cuts for each type of multilepton signal.

4.1 Estimation of the backgrounds to the multilepton signals

In this subsection we obtain rough estimations of the backgrounds to the multilepton signals. For the $3l + \not{E}_T$ signal, we take background obtained by the ATLAS Run II experiment in this channel [16] and scale the number of events for the higher luminosity ($3000\,\mathrm{fb}^{-1}$). For simulating the $3l + \not{E}_T$ signal in a pMSSM, we also follow the procedure of [16]. For other signals namely $4l$, $ss3os1l$ (three same sign and one opposite sign l) and $5l$, suitable cuts are devised to control the SM background in each case (see table 2). The dominant SM processes contributing to the multilepton final states are $t\bar{t}Z$, ZZ and VVV with $V = W^{\pm}, Z$. In table 2 N_l, Q_l are total number of isolated leptons in the final state and their total electric charge respectively and m_{SFOS} is the invariant mass of a pair of same flavour opposite sign (SFOS) lepton pair. The main background in case of $4l + \not{E}_T$ channel comes from pair productions of Z boson and hence the invariant mass cut around the Z-window turns out to be very useful for reducing the background events. As the lepton multiplicity in the final state increases, the backgrounds become weaker and can be adequately suppressed by fewer cuts. For example, for the $5l + \not{E}_T$ signal a moderate cut of $80\,\mathrm{GeV}$ on $\not{E}_T$ is sufficient to make the background negligible.

The total effective cross-section (i.e. the cross-section after all cuts) of the SM backgrounds in the $3l + \not{E}_T$ channel listed in table 2 is $0.261\,\mathrm{fb}$. For the $nl + \not{E}_T$ channels with $n > 3$, the total SM backgrounds are negligible. The strength of each multilepton signal is illustrated by two observables σ_{eff} and N_{BSM} where σ_{eff} is the effective cross-section in the respective channels after passing all cuts and N_{BSM} is the corresponding number of surviving signal events. As a rough guideline we require $N_{\mathrm{BSM}} = 5$ for discovery if the background is negligible. For the $3l + \not{E}_T$ channel, however, we quote the signal significance $S/\sqrt{B}$ where S is the number of signal events and B is the number of corresponding background events which is nonzero.

4.2 Compressed Light Higgsino Heavy Slepton (CLHHS ($\widetilde{W}$)) model

We first present the result of scanning the parameter space of the compressed model (section 2.4, model (2.4 a)) by varying two gaugino masses in figure 2. Along the x-axis $m_{\widetilde{\chi}_2^{\pm}}$ is varied while along the y-axis the variable is $m_{\widetilde{\chi}_1^0}$ which is nearly degenerate with other lighter eweakino masses. The blue (black) contour represents the exclusion coming from $3l + \not{E}_T$ data at 13 (8) TeV [12, 16]. The Run II data rules out a larger part of the parameter space as compared to Run I data. For a LSP of mass around $80\,\mathrm{GeV}$, the bound on $m_{\widetilde{\chi}_2^{\pm}}$ is now extended upto $\approx 800\,\mathrm{GeV}$ (previously it was nearly $600\,\mathrm{GeV}$). Since we
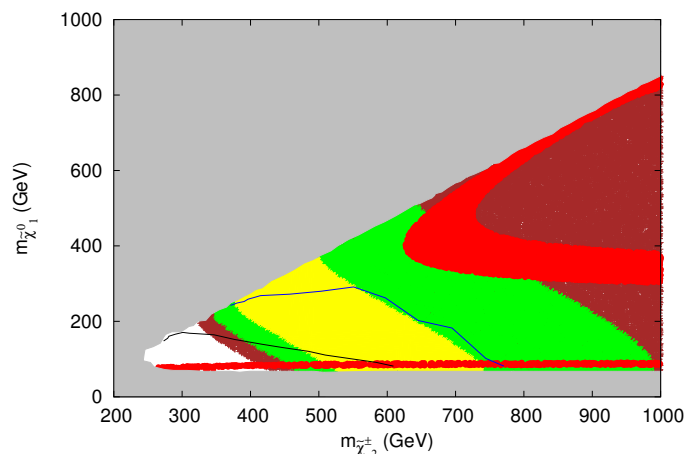
Figure 2. Exclusion contours in the $m_{\widetilde{\chi}_2^\pm} - m_{\widetilde{\chi}_1^0}$ plane in the Compressed Light Higgsino Heavy Slepton (CLHHS $(\widetilde{W})$) model. The blue (black) line represents exclusion obtained by us ([10]) using the ATLAS $3l + \not{E}_T$ search data from Run II (Run I). Colors and conventions are same as in figure 1.

Mass			Cross-section	$3l + \not{E}_T$		$4l + \not{E}_T$		$ss3os1l + \not{E}_T$		$5l + \not{E}_T$	
$m_{\widetilde{\chi}_1^0}$	$m_{\widetilde{\chi}_1^\pm}$	$m_{\widetilde{\chi}_2^\pm}$	in fb	σ_{eff}^{3l}	$(S/\sqrt{B})_{3l}$	σ_{eff}^{4l}	N_{4l}	$\sigma_{\text{eff}}^{ss3os1l}$	$N_{ss3os1l}$	σ_{eff}^{5l}	N_{5l}
249.7	290.2	649.9	156.7	0.0423	13.1	0.0752	225.6	0.0282	84.6	0.0157	47.0
399.9	440.7	650.2	40.14	0.0064	1.9	0.0313	93.9	0.0144	43.3	0.0068	20.5
499.8	527.9	650.3	23.64	0.0054	1.2	0.0147	43.9	0.0083	24.8	0.0033	9.9
199.9	239.8	749.8	298.0	0.0805	24.9	0.0387	116.2	0.0059	17.9	0.0057	17.1
400.7	445.4	750.3	33.42	0.0144	4.4	0.0214	64.2	0.0070	21.1	0.0053	16.1
550.8	591.0	750.3	13.59	0.0031	0.69	0.0098	29.4	0.0043	13.0	0.0024	7.3
300.6	344.4	850.2	80.86	0.0307	9.5	0.0145	43.7	0.004	12.1	0.0032	9.7
400.6	447.1	849.9	30.68	0.0129	3.9	0.0117	34.9	0.0043	12.9	0.0012	3.7
500.2	548.3	850.0	14.40	0.0056	1.7	0.0095	28.5	0.0029	8.6	0.0017	5.2
350.7	376.2	500.3	88.62	0.0195	3.8	0.0691	207.4	0.031	93.1	0.0071	21.3
350.9	393.9	700.4	53.56	0.0198	6.1	0.0348	104.4	0.0134	40.2	0.0075	22.5
350.4	396.0	899.9	47.59	0.0186	5.7	0.0081	24.3	0.0038	11.4	0.0019	5.7

Table 3. The masses and production cross-sections of all possible eweakino pairs for different BPs in the CLHHS $(\widetilde{W})$ model are given. For the trilepton signal in each case we display the significance $(S/\sqrt{B})$. The corresponding σ_{eff} and total number of signal events (with negligible backgrounds) for each type of multilepton signal with $n > 3$ are also shown. Masses and cross-sections are in GeV and fb respectively.

have illustrated the effect of compression by the choice $\mu = 1.05\,M_1$, $m_{\widetilde{\chi}_1^0} < 80\,\text{GeV}$ is not allowed by the LEP lower bound on $m_{\widetilde{\chi}_1^\pm}$ [74]. On the other hand, above $m_{\widetilde{\chi}_1^0} \approx 350\,\text{GeV}$ (which was around 200 GeV for Run I), there is no bound on $m_{\widetilde{\chi}_2^\pm}$. The eweakino search in the $3l + \not{E}_T$ channel at Run II disfavours bulk of the bands allowed by the a_μ constraint at 1σ and 2σ levels for low $m_{\widetilde{\chi}_2^\pm}$. But almost the entire 2σ band in the high $m_{\widetilde{\chi}_2^\pm}$ region survives. Although the red parabolic region allowed by the measured DM relic density remains unaffected by the Run II data, a large part of lower branch is excluded by the same.
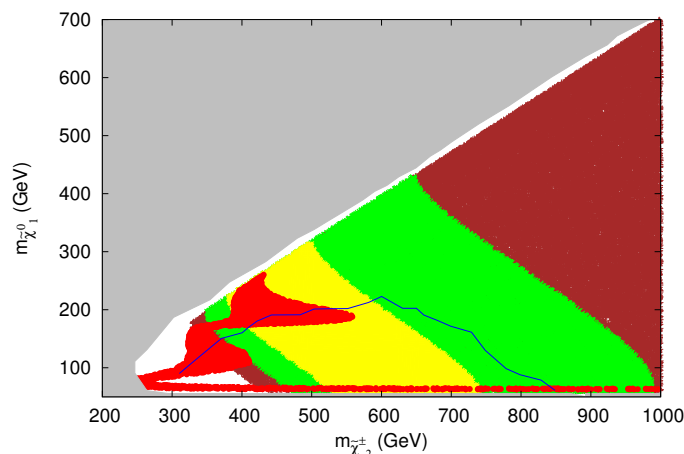
Figure 3. Exclusion contour in the $m_{\widetilde{\chi}_2^\pm} - m_{\widetilde{\chi}_1^0}$ plane in the Moderately Compressed Light Higgsino Heavy Slepton (MCLHHS $(\widetilde{W})$) model. The blue line represents the exclusion obtained by us using the ATLAS $3l + \not{E}_T$ search data from Run II. Colors and conventions are same as in figure 1.

In table 3, we showcase the results of our simulations of multilepton signals at $\sqrt{S} = 13\,\text{TeV}$ for an integrated luminosity of $3000\,\text{fb}^{-1}$ using BPs chosen from the APS. For clarity we have studied four groups of BPs all belonging to the APS shown in figure 2. For the first three groups, $m_{\widetilde{\chi}_2^\pm}$ is fixed at 650, 750 and 850 GeV respectively while $m_{\widetilde{\chi}_1^0}$ is varied. It is important to note that for $m_{\widetilde{\chi}_1^0} > 350\,\text{GeV}$, the trilepton signal is below the observable level ($S/\sqrt{B} < 5$) irrespective of $m_{\widetilde{\chi}_2^\pm}$. In most of such cases one of the multilepton signals with $n > 3$ is likely to be the discovery channel ($N_{\text{BSM}} > 5$). On the other hand the last group of BPs illustrates that the $3l + \not{E}_T$ signal improves for $m_{\widetilde{\chi}_1^0} = 350\,\text{GeV}$ even for $m_{\widetilde{\chi}_2^\pm}$ as high as 900 GeV. Similar features have been observed for the moderately compressed model (see the next subsection).

4.3 Moderately Compressed Light Higgsino Heavy Slepton (MCLHHS $(\widetilde{W})$) model

Figure 3 represents the result of scanning in the $m_{\widetilde{\chi}_2^\pm} - m_{\widetilde{\chi}_1^0}$ plane in the model with moderate compression (model (2.4 b)) illustrated by the choice $\mu = 1.3\,M_1$. The blue line is the exclusion contour coming from the ATLAS $3l + \not{E}_T$ data at Run II. For a LSP with mass around 60 GeV, $m_{\widetilde{\chi}_2^\pm}$ below 850 GeV is disfavoured by the LHC search. LSP mass cannot be lowered further due to the lower bound on $m_{\widetilde{\chi}_1^\pm}$ coming from the LEP [74] data. On the other hand above $m_{\widetilde{\chi}_1^0} \approx 230\,\text{GeV}$, all $\widetilde{\chi}_2^\pm$ masses are allowed.

We pointed out in [10] that by relaxing the compression between μ and M_1, it is possible to get the DM relic density satisfying parameter space for lower values of $m_{\widetilde{\chi}_2^\pm}$ which looks interesting from the perspective of sparticle searches. The red points in figure 3 is consistent with the observed DM relic density of the universe. A significant fraction of the upper red patches lying in the low $m_{\widetilde{\chi}_2^\pm}$ region is indeed allowed by the Run II data. However for the lower red band only the part with $m_{\widetilde{\chi}_2^\pm} \gtrsim 850\,\text{GeV}$ is consistent with present LHC limits. For $m_{\widetilde{\chi}_2^\pm}$ lying approximately in the range 500–600 GeV a significant

Mass			Cross-section	$3l + \not{E}_T$		$4l + \not{E}_T$		$ss3os1l + \not{E}_T$		$5l + \not{E}_T$	
$m_{\widetilde{\chi}_1^0}$	$m_{\widetilde{\chi}_1^\pm}$	$m_{\widetilde{\chi}_2^\pm}$	in fb	$\sigma_{\mathrm{eff}}^{3l}$	$(S/\sqrt{B})_{3l}$	$\sigma_{\mathrm{eff}}^{4l}$	N_{4l}	$\sigma_{\mathrm{eff}}^{ss3os1l}$	$N_{ss3os1l}$	$\sigma_{\mathrm{eff}}^{5l}$	N_{5l}
240.4	325.4	600.0	137.9	0.0469	14.5	0.0579	173.7	0.0152	45.5	0.0096	28.9
300.5	397.3	600.8	74.0	0.0244	6.8	0.0215	64.4	0.0126	37.7	0.0148	44.4
360.2	461.9	600.8	48.98	0.0279	3.9	0.01812	54.4	0.01029	30.8	0.0142	42.6
390.3	484.7	601.2	44.03	0.0136	2.7	0.0172	51.5	0.007	21.1	0.0075	22.4
110.4	166.9	800.4	1249.0	0.1124	34.6	0.0249	74.9	0.0125	37.5	0.0125	37.5
199.9	278.7	800.4	218.3	0.0458	14.1	0.0306	91.7	0.0109	32.7	0.0022	6.5
301.3	406.1	801.4	54.88	0.0324	9.9	0.0082	24.7	0.0021	6.3	0.0033	9.9
400.7	529.7	800.6	20.76	0.0079	2.4	0.0081	24.3	0.0048	14.3	0.0029	8.7
501.5	646.7	800.1	10.7	0.0031	0.86	0.0029	8.9	0.0019	5.8	0.0013	3.8
300.3	371.8	501.1	115.3	0.0265	5.6	0.0507	152.2	0.0165	49.6	0.012133	36.4
300.1	401.1	700.2	58.15	0.0221	6.5	0.0105	31.4	0.0077	23.2	0.0077	23.2
300.6	406.5	900.1	53.21	0.0176	5.4	0.0043	12.8	—	—	0.0016	4.8

Table 4. The masses and production cross-sections of all possible eweakino pairs for different BPs in the MCLHHS ($\widetilde{W}$) model are given. For the trilepton signal in each case we display the significance ($S/\sqrt{B}$). The corresponding σ_{eff} and total number of signal events (with negligible backgrounds) for each type of multilepton signal with $n > 3$ are also shown. Masses and cross-sections are in GeV and fb respectively.

part of the APS is consistent with both DM relic density and a_μ data (at 1σ level). Also the 2σ band of a_μ corresponding to larger values of $m_{\widetilde{\chi}_2^\pm}$ is compatible with the $3l + \not{E}_T$ data.

Table 4 shows the status of multilepton signals for different representative BPs. The BPs are bunched into three groups for reasons discussed in the last subsection. For a $\widetilde{\chi}_2^\pm$ with masses 600 and 800 GeV, the entire range of LSP masses considered gives potential $nl + \not{E}_T$ signals with $n > 3$ for $3000\,\mathrm{fb}^{-1}$ of integrated luminosity. But in most of the cases the trilepton signal is weaker compared to the other multilepton channels. On the other hand keeping LSP mass fixed around 300 GeV, we have also varied $m_{\widetilde{\chi}_2^\pm}$ and found that it is possible to get significantly large $3l + \not{E}_T$ signal even for 900 GeV. Although for $m_{\widetilde{\chi}_2^\pm} = 900\,\mathrm{GeV}$, the $ss3os1l$ and $5l$ signals are already rather weak.

4.4 CLHHS ($\widetilde{B} - \widetilde{W}$) model

The result of scanning the parameter space of this model (model (2.4 c)) is displayed in figure 4. The blue line is the exclusion contour obtained using the ATLAS $3l + \not{E}_T$ search at Run II. The mass of $\widetilde{\chi}_2^\pm$ all the way upto 900 GeV is ruled out by the LHC data for a LSP with mass around 105 GeV. Note that, here LSP mass has a lower bound at around 105 GeV coming from the LEP data. This is because in this model the entire lighter eweakino spectrum is degenerate with mass controlled by higgsino parameter μ and hence the LEP bound on $m_{\widetilde{\chi}_1^\pm}$ is tantamount to a bound on $m_{\widetilde{\chi}_1^0}$ (see subsection 2.4 model (2.4 c)). On the other hand, above $m_{\widetilde{\chi}_1^0} \approx 290\,\mathrm{GeV}$, there is no bound on $m_{\widetilde{\chi}_2^\pm}$.

We also show the 1σ (yellow) and 2σ (green) allowed a_μ bands in the same plot. A fairly large part of these a_μ bands in the APS covering a wide range of $m_{\widetilde{\chi}_2^\pm}$ is consistent with the present LHC Limit. Another point worth noting is that the APS as shown in figure 4 does not contain any region consistent with the DM relic density data. This, however, is not surprising. It is well known that for a higgsino dominated LSP, DM relic density in the right ballpark value can be obtained only for high values of $m_{\widetilde{\chi}_1^0}$ (e.g., $m_{\widetilde{\chi}_1^0}$
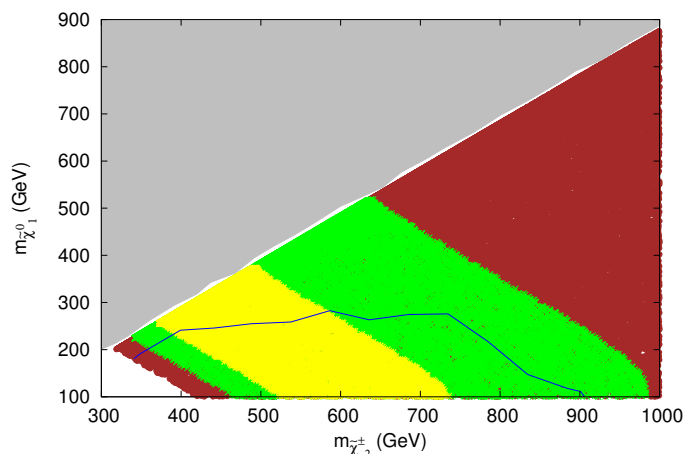
Figure 4. Exclusion contour in the $m_{\widetilde{\chi}_2^\pm} - m_{\widetilde{\chi}_1^0}$ plane in the CLHHS $(\widetilde{B} - \widetilde{W})$ model. The blue line represents exclusion obtained by us using the ATLAS $3l + \not{E}_T$ search data from Run II. Colors and conventions are same as in figure 1.

Mass			Cross-section	$3l + \not{E}_T$		$4l + \not{E}_T$		$ss3os1l + \not{E}_T$		$5l + \not{E}_T$	
$m_{\widetilde{\chi}_1^0}$	$m_{\widetilde{\chi}_1^\pm}$	$m_{\widetilde{\chi}_2^\pm}$	in fb	σ_{eff}^{3l}	$(S/\sqrt{B})_{3l}$	σ_{eff}^{4l}	N_{4l}	$\sigma_{\text{eff}}^{ss3os1l}$	$N_{ss3os1l}$	σ_{eff}^{5l}	N_{5l}
310.1	316.9	600.5	140.31	0.0449	13.8	0.0463	138.9	0.0014	4.2	0.0014	4.2
370.0	377.4	600.1	80.21	0.0104	3.2	0.0216	64.9	0.0016	4.8	—	—
330.2	335.6	700.6	104.88	0.0367	11.3	0.0231	69.2	—	—	—	—
380.2	386.3	700.1	63.55	0.0229	7.1	0.0178	53.4	0.0013	3.8	—	—
430.5	437.2	700.3	41.55	0.0108	3.3	0.0095	28.6	0.0017	4.9	—	—
280.8	289.3	500.1	222.58	0.0356	10.9	0.0935	280.4	0.0044	13.4	—	—
280.1	285.4	700.5	190.24	0.0609	18.7	0.0418	125.6	0.0019	5.7	—	—
280.2	284.8	800.5	186.62	0.0504	15.5	0.0186	55.9	—	—	—	—

Table 5. The masses and production cross-sections of all possible eweakino pairs for different BPs in the CLHHS $(\widetilde{B} - \widetilde{W})$ model are given. For the trilepton signal in each case we display the significance $(S/\sqrt{B})$. The corresponding σ_{eff} and total number of signal events (with negligible backgrounds) for each type of multilepton signal with $n > 3$ are also shown. Masses and cross-sections are in GeV and fb respectively.

around 1 TeV [75, 76] assuming single component DM. Our result agrees with this. In ref. [42], authors have shown that this upper limit for higgsino DM mass can be relaxed if a small amount of slepton co-annihilation is present. Note that in our model such a co-annihilation cannot occur as sleptons are much heavier than the LSP.

In table 5 we present the results of multilepton signals for an integrated luminosity of $3000\,\text{fb}^{-1}$. Our investigation reveals that for $m_{\widetilde{\chi}_2^\pm} \approx 700\,\text{GeV}$, the entire range of $m_{\widetilde{\chi}_1^0}$ in the APS can be probed via $3l + \not{E}_T$ and $4l + \not{E}_T$ channel. Again, for a LSP of mass around $280\,\text{GeV}$, $\widetilde{\chi}_2^\pm$ as heavy as $800\,\text{GeV}$ can lead to observable $3l/4l + \not{E}_T$ signal. However note that, $ss3os1l + \not{E}_T$ and $5l + \not{E}_T$ channels produce weaker signals in most of the cases.

4.5 Light Higgsino and Heavy Slepton (LHHS) model

We delineate the APS of LHHS model (subsection 2.2, model (2.2 b)) in the $m_{\widetilde{\chi}_1^\pm} - m_{\widetilde{\chi}_1^0}$ plane in figure 5. Run II data puts stronger constraint (the blue curve) on the APS
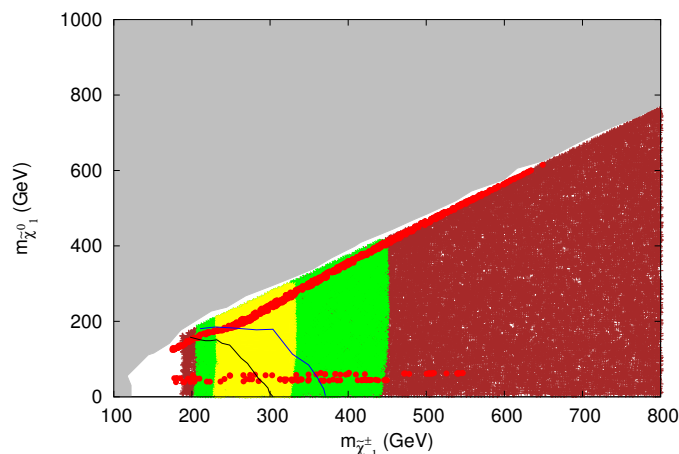
Figure 5. Exclusion contours in the $m_{\widetilde{\chi}_1^\pm} - m_{\widetilde{\chi}_1^0}$ plane in the Light Higgsino and Heavy Slepton (LHHS) model. The blue (black) line represents exclusion obtained by us ([10]) using the ATLAS $3l + \not{E}_T$ search data from Run II (Run I). Colors and conventions are same as in figure 1.

compared to the Run I data (the black curve) [10]. For massless LSP, a $\widetilde{\chi}_1^\pm$ with mass above $\gtrsim 370\,\text{GeV}$ (the corresponding value of $m_{\widetilde{\chi}_2^\pm}$ is $\gtrsim 600\,\text{GeV}$) is allowed whereas above $m_{\widetilde{\chi}_1^0} \approx 200\,\text{GeV}$ there is no bound on $m_{\widetilde{\chi}_1^\pm}$. Run II data eliminates a larger part of the lower DM band originating from h and Z resonances as compared to the Run I data. However almost the entire upper DM band survives except a tiny part. For $m_{\widetilde{\chi}_1^\pm}$ lying in the range 250–450 GeV, a large part of the APS is in agreement with both DM relic density and a_μ data (both at 1σ and 2σ levels).

We exhibit the results of multilepton searches for LHHS model in table 6. The mode of presentation is same as in earlier tables. For a $\widetilde{\chi}_1^\pm$ with mass e.g. say 500 GeV, the entire range of LSP mass 50–450 GeV (see figure 5) allowed by the $3l + \not{E}_T$ data can be probed at the LHC with $\mathcal{L} = 3000\,\text{fb}^{-1}$. On the other hand for a LSP of mass 300 GeV, good signal strength can be expected for almost each type of multilepton signal for $m_{\widetilde{\chi}_1^\pm}$ nearly upto 550 GeV (which corresponds to $m_{\widetilde{\chi}_2^\pm} \approx 900\,\text{GeV}$). In some cases the $3l + \not{E}_T$ signal again turns out to be weaker as compared to channels with higher lepton multiplicities. For higher values of $m_{\widetilde{\chi}_1^\pm}$, multilepton signal especially $ss3os1l$ and $5l$ signals get weaken rapidly. This can be understood easily as follows. In LHHS model, as sleptons masses are put between $m_{\widetilde{\chi}_1^\pm}$ and $m_{\widetilde{\chi}_2^\pm}$ (see subsection 2.2, model (2.2 b)), only $\widetilde{\chi}_2^\pm(\widetilde{\chi}_4^0)$ has direct decays into sleptons while the leptons can come from $\widetilde{\chi}_1^\pm(\widetilde{\chi}_2^0, \widetilde{\chi}_3^0)$ decays via SM gauge bosons with low BR. Therefore, the heavy EW sector is the main source of multileptons in this case. It was shown in [10] explicitly. Now, $m_{\widetilde{\chi}_2^\pm}$ increases with increasing value of $m_{\widetilde{\chi}_1^\pm}$ and that in turn decreases the cross-section of heavy sector. As a result, one starts getting poor signals.

4.6 Light Higgsino and Light Left Slepton (LHLS) Model

We show the exclusion contour (the blue curve) in the $m_{\widetilde{\chi}_1^\pm} - m_{\widetilde{\chi}_1^0}$ plane obtained by scanning the parameter space of the LHLS Model (see section 2.2, model (2.2 a)) in figure 6.

Mass			Cross-section	$3l + \not{E}_T$		$4l + \not{E}_T$		$ss3os1l + \not{E}_T$		$5l + \not{E}_T$	
$m_{\widetilde{\chi}_1^0}$	$m_{\widetilde{\chi}_1^\pm}$	$m_{\widetilde{\chi}_2^\pm}$	in fb	σ_{eff}^{3l}	$(S/\sqrt{B})_{3l}$	σ_{eff}^{4l}	N_{4l}	$\sigma_{\text{eff}}^{ss3os1l}$	$N_{ss3os1l}$	σ_{eff}^{5l}	N_{5l}
40.7	380.7	620.3	86.86	0.0669	20.6	0.0269	80.8	0.0165	49.5	0.0043	13.0
159.7	380.7	620.3	86.16	0.0534	16.4	0.0293	87.8	0.012	36.2	0.0103	31.0
321.3	380.7	620.3	74.43	0.0231	7.1	0.0372	111.6	0.0067	20.1	0.0082	24.6
49.98	500.8	795.9	26.57	0.0268	8.3	0.0074	22.3	0.0039	11.9	0.0027	7.9
199.7	500.8	795.9	26.48	0.0244	7.5	0.0087	26.2	0.0045	13.5	0.0026	7.8
400.3	500.8	795.9	25.64	0.0128	3.8	0.0053	15.8	0.0015	4.5	0.0035	10.5
300.4	350.7	576.9	99.23	0.0288	7.9	0.0635	190.5	0.0228	68.5	0.0039	11.9
300.3	449.6	720.8	41.73	0.0196	6.1	0.0108	32.5	0.0033	10.0	0.0037	11.3
300.4	550.7	869.6	17.07	0.0145	4.4	0.0051	15.4	0.0027	8.2	0.0005	1.5

Table 6. The masses and production cross-sections of all possible eweakino pairs for different BPs in the LHHS model are given. For the trilepton signal in each case we display the significance $(S/\sqrt{B})$. The corresponding σ_{eff} and total number of signal events (with negligible backgrounds) for each type of multilepton signal with $n > 3$ are also shown. Masses and cross-sections are in GeV and fb respectively.

The choice of the L-slepton masses is as in section 2.2. The constraints are significantly stronger than the ones obtained from the Run I data (the black curve) [10]. For example, the lower bound on $m_{\widetilde{\chi}_1^\pm}$ for a LSP with negligible mass is now extended from 450 GeV (Run I) to 650 GeV. The corresponding lower bound on $m_{\widetilde{\chi}_2^\pm}$ is ≈ 1.01 TeV. Above $m_{\widetilde{\chi}_1^0} \simeq$ 300 GeV, there is no bound on $m_{\widetilde{\chi}_1^\pm}$. In addition one can also put correlated bounds on $m_{\widetilde{\chi}_1^\pm}$ and $m_{\widetilde{\chi}_1^0}$ coming from ATLAS slepton search[3] at Run II [16] of the LHC (see the magenta curve in figure 6). It is interesting to note that the bound on $m_{\widetilde{\chi}_1^\pm}$ for a massless LSP as obtained from the slepton search is around 1 TeV which is much stronger than that coming from direct eweakino searches at Run II.

The exclusion using Run II data depletes the bands allowed by the a_μ data severely leaving only a small fraction of the green 2σ band within the APS. The lower branch of the red region allowed by the DM relic density constraint, a part of which was allowed by the LHC Run I eweakino searches, are now excluded by the Run II data. This has implications for the compatibility of this model and the DM direct detection data taken at its face value (see below). A significant portion of the upper red branch is still allowed.

Various multilepton signals in this model for an integrated luminosity of 3000 fb^{-1} are displayed in table 7. The $3l+\not{E}_T$ signal is observable for almost the full set of BPs considered here. It also follows that N_{BSM} exceeds 5 for all signals with $n \geq 3$ for a relatively low $m_{\widetilde{\chi}_1^\pm} = 480$ GeV for several choices of the LSP mass. However as $m_{\widetilde{\chi}_1^\pm}$ increases to 600 GeV, the cross-section for heavy eweakino pair production decreases rapidly (for this value of $m_{\widetilde{\chi}_1^\pm}$, we have $m_{\widetilde{\chi}_2^\pm}(m_{\widetilde{\chi}_4^0}) \approx 940$ GeV). The $ss3os1l$ and $5l$ signals that mainly come from heavy eweakino productions become weaker. The same features are seen when we vary $m_{\widetilde{\chi}_1^\pm}$ keeping $m_{\widetilde{\chi}_1^0}$ fixed at 400 GeV. For the entire range considered by us the $4l + \not{E}_T$ signal, which is not very common in the corresponding model with decoupled heavier eweakinos, is observable.

---

[3]The slepton mass in the LHLS model is related to $m_{\widetilde{\chi}_1^\pm}$ and $m_{\widetilde{\chi}_1^0}$ through the assumption $m_{\tilde{l}_L} = \frac{m_{\widetilde{\chi}_1^\pm} + m_{\widetilde{\chi}_1^0}}{2}$.
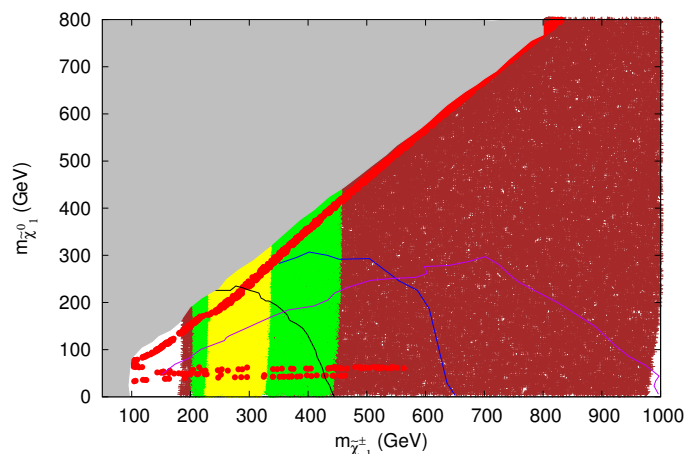
Figure 6. Exclusion contours in the $m_{\widetilde{\chi}_1^\pm} - m_{\widetilde{\chi}_1^0}$ plane in the Light Higgsino and Light Left Slepton (LHLS) model. The blue (black) line represents exclusion obtained by us ([10]) using the ATLAS $3l + \not{E}_T$ search data from Run II (Run I). The exclusion from the direct slepton search (the magenta curve) is also shown. Colors and conventions are same as in figure 1.

Mass			Cross-section	$3l + \not{E}_T$		$4l + \not{E}_T$		$ss3os1l + \not{E}_T$		$5l + \not{E}_T$	
$m_{\widetilde{\chi}_1^0}$	$m_{\widetilde{\chi}_1^\pm}$	$m_{\widetilde{\chi}_2^\pm}$	in fb	σ_{eff}^{3l}	$(S/\sqrt{B})_{3l}$	σ_{eff}^{4l}	N_{4l}	$\sigma_{\text{eff}}^{ss3os1l}$	$N_{ss3os1l}$	σ_{eff}^{5l}	N_{5l}
309.9	480.2	763.6	31.42	0.0638	19.6	0.0223	66.9	0.0047	14.1	0.0028	8.5
359.8	480.2	763.6	30.76	0.0489	13.5	0.0225	67.4	0.0065	19.4	0.0037	11.1
410.1	480.3	763.8	28.62	0.0641	9.1	0.0346	103.9	0.0077	23.2	0.0054	16.3
259.6	600.4	940.5	11.41	0.0604	18.5	0.0073	21.9	0.0008	2.4	0.0009	2.7
349.8	600.4	940.5	11.29	0.0387	11.9	0.0048	14.6	0.0009	2.7	0.0008	2.0
550.2	600.5	940.9	9.252	0.0149	2.1	0.0077	23.0	0.0018	5.3	0.0012	3.6
400.1	450.6	720.4	34.67	0.0368	8.1	0.0319	95.7	0.0055	16.6	0.0028	8.3
400.4	549.6	865.6	16.82	0.0225	6.3	0.0056	16.7	0.0012	3.5	0.0015	4.5
400.5	650.1	1014.0	7.68	0.0230	7.1	0.0039	11.7	0.0008	2.5	0.0002	0.5

Table 7. The masses and production cross-sections of all possible eweakino pairs for different BPs in the LHLS model are given. For the trilepton signal in each case we display the significance $(S/\sqrt{B})$. The corresponding σ_{eff} and total number of signal events (with negligible backgrounds) for each type of multilepton signal with $n > 3$ are also shown. Masses and cross-sections are in GeV and fb respectively.

4.7 Light Mixed and Light Left Slepton (LMLS) model

The APS of the LMLS model in the $m_{\widetilde{\chi}_1^\pm} - m_{\widetilde{\chi}_1^0}$ plane consistent with all constraints is shown in figure 7. The parameter space is tightly constrained in this case. The bound on $m_{\widetilde{\chi}_1^\pm}$ for a massless LSP coming from the Run II data (the blue curve) is $\approx 960\,\text{GeV}$. This limit on $m_{\widetilde{\chi}_1^\pm}$ differs from that in case of Run I (the black curve) [10] by atleast $300\,\text{GeV}$. On the other hand above $m_{\widetilde{\chi}_1^0} = 450\,\text{GeV}$, the LHC puts no constraint on the mass of $\widetilde{\chi}_2^\pm$. The magenta line represents the exclusion limit on $m_{\widetilde{\chi}_1^\pm}$ as a function of LSP mass coming from the LHC slepton search [16]. The present LHC limits affect severely the part of the APS which is consistent with both DM relic density and a_μ data over a small region. A small part of 1σ and 2σ allowed a_μ bands lies beyond the Run II exclusion contour. The APS with $m_{\widetilde{\chi}_1^\pm}$ in the range 350 - 600 GeV is phenomenologically very interesting as it is
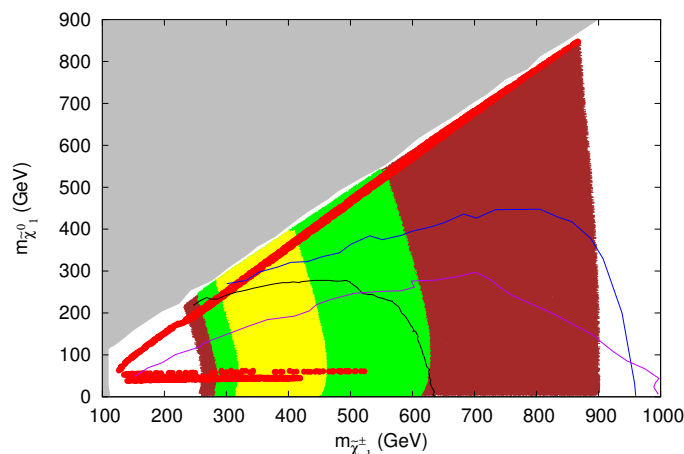
Figure 7. Exclusion contours in the $m_{\widetilde{\chi}_1^\pm} - m_{\widetilde{\chi}_1^0}$ plane in the Light Mixed and Light Left Slepton (LMLS) model. The blue (black) line represents exclusion obtained by us [10] using the ATLAS $3l + \not{E}_T$ search data from Run II (Run I). The exclusion from the direct slepton search (the magenta curve) is also shown. Colors and conventions are same as in figure 1.

allowed by both DM relic density and a_μ data. Although the upper DM band extends upto $m_{\widetilde{\chi}_1^\pm} \approx 900\,\mathrm{GeV}$, the region with high $m_{\widetilde{\chi}_1^\pm}$ is likely to give poor multilepton signal at the high luminosity LHC (see below). Note that, the lower DM band was already ruled out by the Run I search.

Table 8 represents the result of multilepton signals in the LMLS model with the help of several BPs. For $m_{\widetilde{\chi}_1^\pm} = 550\,\mathrm{GeV}$, the entire allowed range of LSP masses (see figure 7) may be probed through multilepton channels with an integrated luminosity of $3000\,\mathrm{fb}^{-1}$. In fact, even the channels like $ss3os1l + \not{E}_T, 5l + \not{E}_T$ which are unique features of non-decoupled heavy eweakinos yield large signals. For higher values of $m_{\widetilde{\chi}_1^\pm}$ (e.g. say $750\,\mathrm{GeV}$), however, $ss3os1l$ and $5l$ signals are poor even with $\mathcal{L} = 3000\,\mathrm{fb}^{-1}$. This again mainly happens due to large masses of the heavier eweakino sector that result into low cross-section. We get the same result when we vary $m_{\widetilde{\chi}_1^\pm}$ keeping LSP mass fixed at a particular value (say $500\,\mathrm{GeV}$). The $4l + \not{E}_T$ channel turns out to be the most promising for the rest of the BPs.

5 Constraints from dark matter direct detection experiments

In this section we study the models constrained in section 4 in the light of the measured spin-independent DM nucleon scattering cross-section (σ_{SI}) by XENON1T [55], LUX [54] and Panda [56] experiments. However, in view of large uncertainties in the computation of σ_{SI} due to theoretical as well as experimental inputs (see section 3), the relatively small differences between them are not very significant. From our scanning we take the points from the APS of each model, compute σ_{SI} for them and compare the results with the upper bounds on σ_{SI}. Our results are shown in figures 7, 8 and 9. In all figures the black curve represents the upper bound on σ_{SI} as a function of the DM mass as obtained by the XENON1T experiment. The green and yellow regions represent 1σ and 2σ sensitivity bands respectively. The large widths of these bands reflect the statistical fluctuations in a typical

Mass			Cross-section	$3l + \not{E}_T$		$4l + \not{E}_T$		$ss3os1l + \not{E}_T$		$5l + \not{E}_T$	
$m_{\widetilde{\chi}_1^0}$	$m_{\widetilde{\chi}_1^\pm}$	$m_{\widetilde{\chi}_2^\pm}$	in fb	$\sigma_{\mathrm{eff}}^{3l}$	$(S/\sqrt{B})_{3l}$	$\sigma_{\mathrm{eff}}^{4l}$	N_{4l}	$\sigma_{\mathrm{eff}}^{ss3os1l}$	$N_{ss3os1l}$	$\sigma_{\mathrm{eff}}^{5l}$	N_{5l}
400.0	550.1	664.3	26.18	0.0688	19.1	0.0259	77.7	0.0034	10.2	0.006	18.1
459.8	550.4	664.5	25.76	0.0551	10.9	0.0227	68.0	0.0059	17.8	0.0049	14.7
520.5	550.7	664.8	22.32	0.0112	2.5	0.0134	40.2	0.0024	7.4	0.0033	10.0
100.6	750.9	866.1	5.761	0.2898	89.4	0.0074	22.1	0.0005	1.72	0.0006	1.9
300.5	750.3	865.3	5.809	0.1922	59.2	0.0084	25.1	0.0006	1.74	0.0009	2.6
499.9	750.0	864.8	5.813	0.0532	16.4	0.007	21.1	0.0006	1.92	0.0011	3.3
699.8	750.9	865.5	5.464	0.0102	2.2	0.0074	22.3	0.0012	3.6	0.0015	4.6
500.0	530.1	644.5	26.44	0.0148	3.3	0.0148	44.4	0.0042	12.7	0.0032	9.5
499.9	629.8	744.2	13.92	0.0339	6.7	0.0128	38.4	0.0019	5.8	0.004	12.1
500.1	829.9	945.1	3.342	0.0177	2.5	0.0049	14.8	0.0005	1.4	0.0004	1.3

Table 8. The masses and production cross-sections of all possible eweakino pairs for different BPs in the LMLS model are given. For the trilepton signal in each case we display the significance $(S/\sqrt{B})$. The corresponding σ_{eff} and total number of signal events (with negligible backgrounds) for each type of multilepton signal with $n > 3$ are also shown. Masses and cross-sections are in GeV and fb respectively.
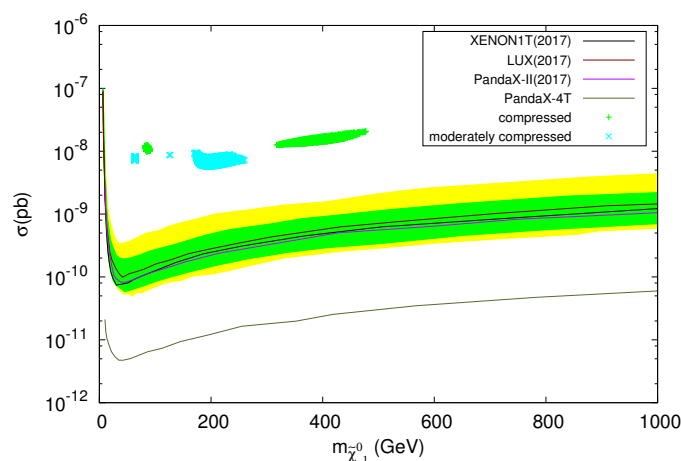

Figure 8. Plot of spin-independent scattering cross-section σ^{SI} for scattering of proton with $\widetilde{\chi}_1^0$ as a function of the LSP mass for the compressed models ((2.4 a), (2.4 b) and (2.4 c)). Only the points which satisfy WMAP/PLANCK, a_μ upto the level of 2σ and the LHC Run II constraints are used in the calculation. The exclusion contours for XENON1T, LUX, PandaX-II and PandaX-4T experiments are shown as black, red, magenta and green lines respectively. In green and yellow are shown 1σ and 2σ sensitivity bands respectively of the XENON1T data.

low count experiment. The lowest curve shows the projected sensitivity of the PandaX-4T experiment [77], which will be operational after the ongoing PandaX -II experiment.

It follows from figure 8 that both the compressed (CLHHS ($\tilde{W}$)) and the moderately compressed (MCLHHS ($\tilde{W}$)) models predict σ_{SI} far above the experimental upper bounds. Thus these models can only survive provided the computed values of σ_{SI} are overestimated by a large factor — a possibility that cannot be ruled out a priori. This can happen if e.g., the DM density in the neighbourhood of the earth, which has not been directly measured, turns out to be unexpectedly small. It may be recalled that only the average value of this
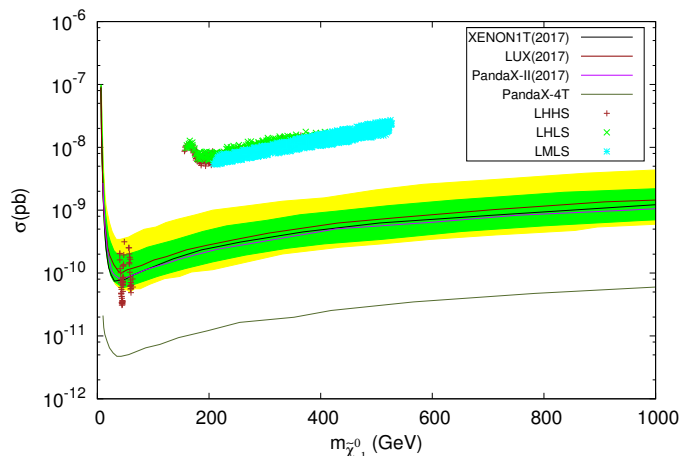
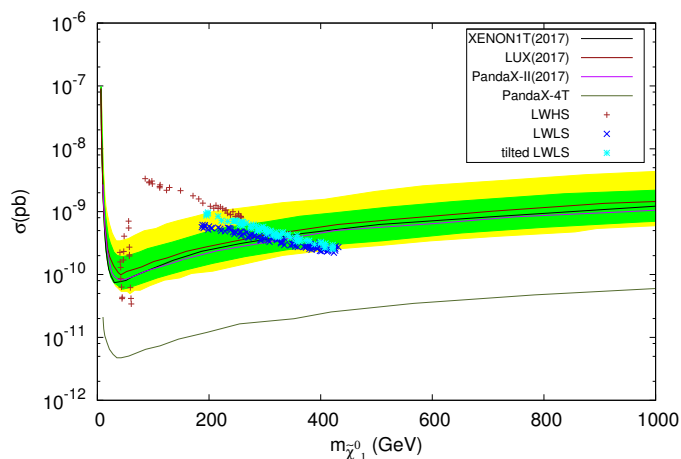**Figure 9**. Same as in figure 8 but for LHHS, LHLS ans LMLS models.

Figure 10. Same as in figure 8 but for various LW type models.

density over a astronomically large volume with the sun at the centre has been measured experimentally. Other uncertainties as discussed in subsection 3.1 leave open the possibility that $\sigma_{\rm SI}$ could be even further suppressed. Thus conclusions based on figure 8 should not to be taken at their face values.

From figure 9 it can be seen that LHLS and LMLS models are also disfavoured. However they cannot be ruled out with confidence thanks to the uncertainties in the computation of $\sigma_{\rm SI}$ as discussed in the last paragraph. It is interesting to note that the LHHS model is still consistent with the DM direct detection data even if figure 9 is taken at its face value. This happens in a part of the APS where the DM relic density is produced by the LSP pair annihilation into the Higgs boson. Similar parameter spaces in other models are now ruled out by the LHC Run II data.

We also note in passing that several LW models are also consistent with the direct detection data (see figure 10).

6 Conclusions

In conclusion we reiterate that the search for the heavier eweakinos could be an important programme at the LHC after the current long shutdown. The searches for the hadronically quiet multilepton ($nl + \not{E}_T$, $n > 3$) signals may even be the SUSY discovery channels if the lighter eweakinos have a compressed spectrum.

In order to reach this conclusion we have carried out the following analyses. We first constrain the full eweakino sector of several generic pMSSMs, described in section 2, using the ATLAS model independent upper bound on the number of any BSM event from trilepton searches at Run II of the LHC [16] (for a summary of models studied in this paper see subsection 2.5 and table 1). We do not employ the often used ad hoc assumption that the heavier eweakinos are decoupled. As explained in section 2 the phenomenology of the heavier eweakinos are particularly important in the light higgsino (LH) models (see subsection 2.2) where they ($\widetilde{\chi}_2^\pm$ and $\widetilde{\chi}_4^0$) are dominantly winos. In this scenario the lighter eweakinos ($\widetilde{\chi}_1^\pm$, $\widetilde{\chi}_2^0$ and $\widetilde{\chi}_3^0$) are higgsino dominated while the LSP is either a higgsino or bino-higgsino admixture. The exclusion contour obtained in a model also depends sensitively on the hierarchy between the slepton and eweakinos masses. Accordingly we have worked in two scenarios i) LHLS (model (2.2 a)) and ii) LHHS models (model (2.2 b)). In addition we have also considered the LMLS model (section 2.3) where the lighter and heavier eweakinos — other than the LSP — are admixtures of wino and higgsino eigenstates. For the smallest allowed LSP mass in each model the lower bounds on $m_{\widetilde{\chi}_1^\pm}$ are 650 GeV (figure 6), 370 GeV (figure 5) and 960 GeV (figure 7) respectively. All of them are significantly weaker than the ATLAS Run II limit of 1150 GeV (see figure 1) for negligible LSP mass obtained in a simplified model similar to the LWLS model (model (2.1 a), subsection 2.1) with decoupled heavier eweakinos. This indicates once more that the prospect of observing interesting physics involving relatively low mass eweakinos in the LH models looks brighter. The corresponding limits on $m_{\widetilde{\chi}_2^\pm}$ are 1.01 TeV, 600 GeV and 1.07 TeV respectively. It also follows that the weakest exclusion from the LHC Run II data occurs in the LHHS model. As a result the APS, consistent with all constraints discussed in section 3.1, is quite large in this model. We also note in passing that the prediction of this model for $\sigma_{\rm SI}$ is consistent with all DM direct detection data (section 5).

It was emphasized in refs. [9, 10] based on the ATLAS Run I data that the heavier eweakinos attain special significance if the lighter eweakino spectrum is compressed so that only weak signals involving mostly soft particles can emanate from them. Keeping this in view we have studied three compressed models i) CLHHS ($\widetilde{W}$) model (model (2.3 a), section 2.4), ii) MCLHHS ($\widetilde{W}$) (model (2.3 b), section 2.4) and iii) CLHHS ($\widetilde{W} - \widetilde{B}$) (model (2.3 c), section 2.4). The exclusion contour and the APS for each model using the ATLAS Run II data are shown in figures 2, 3 and 4 respectively. For the lowest LSP mass allowed by the LEP data, the lower bounds on $m_{\widetilde{\chi}_2^\pm}$ in these compressed models are 775 GeV, 850 GeV and 900 GeV respectively. On the other hand there is no constraint even from the Run II data for LSP masses above 200–300 GeV in any of these three compressed model.

The prospects of observing multilepton ($nl + \not{E}_T$, $n = 3, 4, 5$) signatures at the high luminosity LHC ($3000\,{\rm fb}^{-1}$) in different models are shown in tables 3–8 using BPs. These

points belong to the APS of the respective models constrained as described above. As already noted, in the compressed models (see tables 3–5) the signals for n = 3 turn out to be rather poor especially for relatively high LSP masses (> 350–400 GeV). In such cases one of the search channels with $n > 3$ could be the discovery channel even for higher LSP masses. In particular the signal with n = 4 appears to be rather promising. Depending on the LSP mass, $m_{\widetilde{\chi}_2^\pm}$ upto 1 TeV can be probed. For the non-compressed model all multilepton channels appear to be relevant provided the LSP mass is around 400–450 GeV or smaller (see tables 6–8).

As discussed in section 5 the LHHS model deserves some attention since it's prediction for $\sigma_{\rm SI}$, taken at its face value, is consistent with the upper bound on this cross-section measured by the DM direct detection experiments [54–56] (figure 8). The predictions of all other LH type models violate the above bound by large factors (see figures 8, 9). We note in passing that the LW type models look better in this respect (see figure 10). Whether the computed $\sigma_{\rm SI}$ should be taken at its face value is, however, not at all clear. This is because of several inputs in the calculation which involve large uncertainties (see subsection 3.1 and references there in). We, therefore, refrain from spelling the final verdict based on the experimental upper bound on $\sigma_{\rm SI}$.

Acknowledgments

References

[1] H.P. Nilles, *Supersymmetry, supergravity and particle physics*, *Phys. Rept.* **110** (1984) 1 [INSPIRE].

[2] H.E. Haber and G.L. Kane, *The search for supersymmetry: probing physics beyond the standard model*, *Phys. Rept.* **117** (1985) 75 [INSPIRE].

[3] S.P. Martin, *A supersymmetry primer*, *Adv. Ser. Direct. High Energy Phys.* **21** (2010) 1 [*Adv. Ser. Direct. High Energy Phys.* **18** (1998) 1] [hep-ph/9709356] [INSPIRE].

[4] D.J.H. Chung et al., *The soft supersymmetry breaking lagrangian: theory and applications*, *Phys. Rept.* **407** (2005) 1 [hep-ph/0312378] [INSPIRE].

[5] M. Drees, P. Roy and R.M. Godbole, *Theory and phenomenology of sparticles*, World Scientific, Singapore (2005).

[6] H. Baer and X. Tata, *Weak scale supersymmetry: from superfields to scattering events*, Cambridge University Press, Cambridge U.K. (2006).

[7] https://twiki.cern.ch/twiki/bin/view/AtlasPublic/SupersymmetryPublicResults

[8] https://twiki.cern.ch/twiki/bin/view/CMSPublic/PhysicsResultsSUS

[9] A. Datta, N. Ganguly and S. Poddar, *New limits on heavier electroweakinos and their LHC signatures*, *Phys. Lett.* **B 763** (2016) 213 [arXiv:1606.04391] [InSPIRE].

[10] M. Chakraborti, A. Datta, N. Ganguly and S. Poddar, *Multilepton signals of heavier electroweakinos at the LHC*, *JHEP* **11** (2017) 117 [arXiv:1707.04410] [InSPIRE].

[11] ATLAS collaboration, *Search for direct production of charginos and neutralinos in events with three leptons and missing transverse momentum in $\sqrt{s} = 8$ TeV pp collisions with the ATLAS detector*, *JHEP* **04** (2014) 169 [arXiv:1402.7029] [InSPIRE].

[12] ATLAS collaboration, *Search for direct production of charginos, neutralinos and sleptons in final states with two leptons and missing transverse momentum in pp collisions at $\sqrt{s} = 8$ TeV with the ATLAS detector*, *JHEP* **05** (2014) 071 [arXiv:1403.5294] [InSPIRE].

[13] CMS collaboration, *Searches for electroweak production of charginos, neutralinos and sleptons decaying to leptons and W, Z and Higgs bosons in pp collisions at 8 TeV*, *Eur. Phys. J.* **C 74** (2014) 3036 [arXiv:1405.7570] [InSPIRE].

[14] CMS collaboration, *Searches for electroweak neutralino and chargino production in channels with Higgs, Z and W bosons in pp collisions at 8 TeV*, *Phys. Rev.* **D 90** (2014) 092007 [arXiv:1409.3168] [InSPIRE].

[15] CMS collaboration, *Search for electroweak production of charginos and neutralinos in multilepton final states in proton-proton collisions at $\sqrt{s} = 13$ TeV*, *JHEP* **03** (2018) 166 [arXiv:1709.05406] [InSPIRE].

[16] ATLAS collaboration, *Search for electroweak production of supersymmetric particles in final states with two or three leptons at $\sqrt{s} = 13$ TeV with the ATLAS detector*, *Eur. Phys. J.* **C 78** (2018) 995 [arXiv:1803.02762] [InSPIRE].

[17] M. Chakraborti et al., *The electroweak sector of the pMSSM in the Light of LHC — 8 TeV and other data*, *JHEP* **07** (2014) 019 [arXiv:1404.4841] [InSPIRE].

[18] M. Chakraborti et al., *Reduced LHC constraints for higgsino-like heavier electroweakinos*, *JHEP* **11** (2015) 050 [arXiv:1507.01395] [InSPIRE].

[19] MSSM WORKING GROUP collaboration, *The minimal supersymmetric standard model: group summary report*, hep-ph/9901246 [InSPIRE].

[20] A. Choudhury and S. Mondal, *Revisiting the exclusion limits from direct chargino-neutralino production at the LHC*, *Phys. Rev.* **D 94** (2016) 055024 [arXiv:1603.05502] [InSPIRE].

[21] A. Choudhury and A. Datta, *Neutralino dark matter confronted by the LHC constraints on electroweak SUSY signals*, *JHEP* **09** (2013) 119 [arXiv:1305.0928] [InSPIRE].

[22] J. Eckel, M.J. Ramsey-Musolf, W. Shepherd and S. Su, *Impact of LSP character on slepton reach at the LHC*, *JHEP* **11** (2014) 117 [arXiv:1408.2841] [InSPIRE].

[23] C. Han, L. Wu, J.M. Yang, M. Zhang and Y. Zhang, *New approach for detecting a compressed bino/wino at the LHC*, *Phys. Rev.* **D 91** (2015) 055030 [arXiv:1409.4533] [InSPIRE].

[24] C. Han, *Probing light bino and higgsinos at the LHC*, *Int. J. Mod. Phys.* **A 32** (2017) 1745003 [arXiv:1409.7000] [InSPIRE].

[25] R.K. Barman, B. Bhattacherjee, A. Chakraborty and A. Choudhury, *Study of MSSM heavy Higgs bosons decaying into charginos and neutralinos*, *Phys. Rev.* **D 94** (2016) 075013 [arXiv:1607.00676] [InSPIRE].

[26] T.A.W. Martin and D. Morrissey, *Electroweakino constraints from LHC data*, *JHEP* **12** (2014) 168 [arXiv:1409.6322] [InSPIRE].

[27] C. Arina, M. Chala, V. Martin-Lozano and G. Nardini, *Confronting SUSY models with LHC data via electroweakino production*, *JHEP* **12** (2016) 149 [arXiv:1610.03822] [ɪɴSPIRE].

[28] GAMBIT collaboration, *Combined collider constraints on neutralinos and charginos*, arXiv:1809.02097 [ɪɴSPIRE].

[29] WMAP collaboration, *Nine-year Wilkinson Microwave Anisotropy Probe (WMAP) observations: cosmological parameter results*, *Astrophys. J. Suppl.* **208** (2013) 19 [arXiv:1212.5226] [ɪɴSPIRE].

[30] PLANCK collaboration, *Planck 2015 results. XIII. Cosmological parameters*, *Astron. Astrophys.* **594** (2016) A13 [arXiv:1502.01589] [ɪɴSPIRE].

[31] H. Baer and X. Tata, *Dark matter and the LHC*, in *Physics at the Large Hadron Collider*, A. Datta et al. eds., Springer, Germany (2009), arXiv:0805.1905 [ɪɴSPIRE].

[32] L. Calibbi, J.M. Lindert, T. Ota and Y. Takanishi, *Cornering light neutralino dark matter at the LHC*, *JHEP* **10** (2013) 132 [arXiv:1307.4119] [ɪɴSPIRE].

[33] M. Demirci and A.I. Ahmadov, *Search for neutralino pair production at the CERN LHC*, *Phys. Rev.* **D 89** (2014) 075015 [arXiv:1404.0550] [ɪɴSPIRE].

[34] L. Calibbi, J.M. Lindert, T. Ota and Y. Takanishi, *LHC tests of light neutralino dark matter without light sfermions*, *JHEP* **11** (2014) 106 [arXiv:1410.5730] [ɪɴSPIRE].

[35] L. Roszkowski, E.M. Sessolo and A.J. Williams, *Prospects for dark matter searches in the pMSSM*, *JHEP* **02** (2015) 014 [arXiv:1411.5214] [ɪɴSPIRE].

[36] J. Bramante et al., *Relic neutralino surface at a 100 TeV collider*, *Phys. Rev.* **D 91** (2015) 054015 [arXiv:1412.4789] [ɪɴSPIRE].

[37] A. Choudhury et al., *Less-simplified models of dark matter for direct detection and the LHC*, *JHEP* **04** (2016) 182 [arXiv:1509.05771] [ɪɴSPIRE].

[38] J. Bramante et al., *Towards the final word on neutralino dark matter*, *Phys. Rev.* **D 93** (2016) 063525 [arXiv:1510.03460] [ɪɴSPIRE].

[39] K. Hamaguchi and K. Ishikawa, *Prospects for Higgs- and Z-resonant neutralino dark matter*, *Phys. Rev.* **D 93** (2016) 055009 [arXiv:1510.05378] [ɪɴSPIRE].

[40] J. Cao et al., *Testing the light dark matter scenario of the MSSM at the LHC*, *JHEP* **03** (2016) 207 [arXiv:1511.05386] [ɪɴSPIRE].

[41] U. Chattopadhyay and A. Dey, *Probing non-holomorphic MSSM via precision constraints, dark matter and LHC data*, *JHEP* **10** (2016) 027 [arXiv:1604.06367] [ɪɴSPIRE].

[42] M. Chakraborti, U. Chattopadhyay and S. Poddar, *How light a higgsino or a wino dark matter can become in a compressed scenario of MSSM*, *JHEP* **09** (2017) 064 [arXiv:1702.03954] [ɪɴSPIRE].

[43] M. Abdughani, L. Wu and J.M. Yang, *Status and prospects of light bino–higgsino dark matter in natural SUSY*, *Eur. Phys. J.* **C 78** (2018) 4 [arXiv:1705.09164] [ɪɴSPIRE].

[44] MUON G-2 collaboration, *Final report of the muon E821 anomalous magnetic moment measurement at BNL*, *Phys. Rev.* **D 73** (2006) 072003 [hep-ex/0602035] [ɪɴSPIRE].

[45] B.L. Roberts, *Status of the Fermilab muon (g − 2) experiment*, *Chin. Phys.* **C 34** (2010) 741 [arXiv:1001.2898] [ɪɴSPIRE].

[46] F. Jegerlehner and A. Nyffeler, *The muon g − 2*, *Phys. Rept.* **477** (2009) 1 [arXiv:0902.3360] [ɪɴSPIRE].

[47] K. Hagiwara, R. Liao, A.D. Martin, D. Nomura and T. Teubner, $(g − 2)_\mu$ and $\alpha(M_Z^2)$ re-evaluated using new precise data, *J. Phys.* **G 38** (2011) 085003 [`arXiv:1105.3149`] [ɪɴSPIRE].

[48] N. Sakai, *Naturalness in supersymmetric guts*, *Z. Phys.* **C 11** (1981) 153 [ɪɴSPIRE].

[49] R.K. Kaul and P. Majumdar, *Cancellation of quadratically divergent mass corrections in globally supersymmetric spontaneously broken gauge theories*, *Nucl. Phys.* **B 199** (1982) 36 [ɪɴSPIRE].

[50] R. Barbieri and G.F. Giudice, *Upper bounds on supersymmetric particle masses*, *Nucl. Phys.* **B 306** (1988) 63 [ɪɴSPIRE].

[51] J.L. Feng, *Naturalness and the status of supersymmetry*, *Ann. Rev. Nucl. Part. Sci.* **63** (2013) 351 [`arXiv:1302.6587`] [ɪɴSPIRE].

[52] A. Djouadi, *The anatomy of electro-weak symmetry breaking. II. The Higgs bosons in the minimal supersymmetric model*, *Phys. Rept.* **459** (2008) 1 [`hep-ph/0503173`] [ɪɴSPIRE].

[53] P. Bechtle et al., *The Light and Heavy Higgs Interpretation of the MSSM*, *Eur. Phys. J.* **C 77** (2017) 67 [`arXiv:1608.00638`] [ɪɴSPIRE].

[54] LUX collaboration, *Results from a search for dark matter in the complete LUX exposure*, *Phys. Rev. Lett.* **118** (2017) 021303 [`arXiv:1608.07648`] [ɪɴSPIRE].

[55] XENON collaboration, *First dark matter search results from the XENON1T experiment*, *Phys. Rev. Lett.* **119** (2017) 181301 [`arXiv:1705.06655`] [ɪɴSPIRE].

[56] PandaX-II collaboration, *Dark matter results from 54-ton-day exposure of PandaX-II experiment*, *Phys. Rev. Lett.* **119** (2017) 181302 [`arXiv:1708.06917`] [ɪɴSPIRE].

[57] ATLAS collaboration, *Search for electroweak production of supersymmetric states in scenarios with compressed mass spectra at $\sqrt{s} = 13$ TeV with the ATLAS detector*, *Phys. Rev.* **D 97** (2018) 052010 [`arXiv:1712.08119`] [ɪɴSPIRE].

[58] CMS collaboration, *Search for new physics in events with two soft oppositely charged leptons and missing transverse momentum in proton-proton collisions at $\sqrt{s} = 13$ TeV*, *Phys. Lett.* **B 782** (2018) 440 [`arXiv:1801.01846`] [ɪɴSPIRE].

[59] P. Schwaller and J. Zurita, *Compressed electroweakino spectra at the LHC*, *JHEP* **03** (2014) 060 [`arXiv:1312.7350`] [ɪɴSPIRE].

[60] S. Jager, *Supersymmetry beyond minimal flavour violation*, *Eur. Phys. J.* **C 59** (2009) 497 [`arXiv:0808.2044`] [ɪɴSPIRE].

[61] M. Cacciari, G.P. Salam and G. Soyez, *The anti-k_t jet clustering algorithm*, *JHEP* **04** (2008) 063 [`arXiv:0802.1189`] [ɪɴSPIRE].

[62] A. Choudhury, S. Rao and L. Roszkowski, *Impact of LHC data on muon $g − 2$ solutions in a vectorlike extension of the constrained MSSM*, *Phys. Rev.* **D 96** (2017) 075046 [`arXiv:1708.05675`] [ɪɴSPIRE].

[63] T. Sjöstrand, S. Mrenna and P.Z. Skands, *PYTHIA 6.4 physics and manual*, *JHEP* **05** (2006) 026 [`hep-ph/0603175`] [ɪɴSPIRE].

[64] M.L. Mangano et al., *ALPGEN, a generator for hard multiparton processes in hadronic collisions*, *JHEP* **07** (2003) 001 [`hep-ph/0206293`] [ɪɴSPIRE].

[65] S. Hoeche et al., *Matching parton showers and matrix elements*, [`hep-ph/0602031`] [ɪɴSPIRE].

[66] M.L. Mangano, M. Moretti, F. Piccinini and M. Treccani, *Matching matrix elements and shower evolution for top-quark production in hadronic collisions*, *JHEP* **01** (2007) 013 [`hep-ph/0611129`] [ɪɴSPIRE].

[67] M. Cacciari, G.P. Salam and G. Soyez, *FastJet user manual*, *Eur. Phys. J.* **C 72** (2012) 1896 [`arXiv:1111.6097`] [ɪɴSPIRE].

[68] J. Pumplin et al., *New generation of parton distributions with uncertainties from global QCD analysis*, *JHEP* **07** (2002) 012 [`hep-ph/0201195`] [ɪɴSPIRE].

[69] ATLAS collaboration, *Observation of a new particle in the search for the standard model Higgs boson with the ATLAS detector at the LHC*, *Phys. Lett.* **B 716** (2012) 1 [`arXiv:1207.7214`] [ɪɴSPIRE].

[70] CMS collaboration, *Observation of a new boson at a mass of 125 GeV with the CMS experiment at the LHC*, *Phys. Lett.* **B 716** (2012) 30 [`arXiv:1207.7235`] [ɪɴSPIRE].

[71] A. Djouadi, J.-L. Kneur and G. Moultaka, *SuSpect: a Fortran code for the supersymmetric and Higgs particle spectrum in the MSSM*, *Comput. Phys. Commun.* **176** (2007) 426 [`hep-ph/0211331`] [ɪɴSPIRE].

[72] A. Djouadi, M.M. Muhlleitner and M. Spira, *Decays of supersymmetric particles: The Program SUSY-HIT (SUspect-SdecaY-HDECAY-InTerface)*, *Acta Phys. Polon.* **B 38** (2007) 635 [`hep-ph/0609292`] [ɪɴSPIRE].

[73] G. Bélanger, F. Boudjema, A. Pukhov and A. Semenov, *MicrOMEGAs_3: a program for calculating dark matter observables*, *Comput. Phys. Commun.* **185** (2014) 960 [`arXiv:1305.0237`] [ɪɴSPIRE].

[74] *The LEP SUSY Working Group*, http://lepsusy.web.cern.ch/lepsusy/.

[75] U. Chattopadhyay, A. Corsetti and P. Nath, *WMAP constraints, SUSY dark matter and implications for the direct detection of SUSY*, *Phys. Rev.* **D 68** (2003) 035005 [`hep-ph/0303201`] [ɪɴSPIRE].

[76] S. Akula, M. Liu, P. Nath and G. Peim, *Naturalness, supersymmetry and implications for LHC and dark Matter*, *Phys. Lett.* **B 709** (2012) 192 [`arXiv:1111.4589`] [ɪɴSPIRE].

[77] PandaX collaboration, *Dark matter direct search sensitivity of the PandaX-4T experiment*, *Sci. China Phys. Mech. Astron.* **62** (2019) 31011 [`arXiv:1806.02229`] [ɪɴSPIRE].